

# Secondary Optics Design Considerations for SuperFlux LEDs

## Introduction

Secondary optics are those optics which exist outside of the LED package, such as reflector cavities, Fresnel lenses, and pillow lenses. Secondary optics are used to create the desired appearance and beam pattern of the LED signal lamp.

The following section details the optical characteristics and optical model creation for Lumileds SuperFlux LEDs. In addition, simple techniques to aid in the design of collimating reflectors, collimating lenses, and pillow lenses are discussed.

## Table of Contents

Introduction .....	1
1. Optical Characteristics of SuperFlux LEDs .....	2
1.1 LED Light Output .....	2
1.2 SuperFlux LED Radiation Patterns .....	2
2. Optical Modeling of SuperFlux LEDs .....	3
2.1 Point Source Optical Model .....	3
2.2 Detailed Optical Models .....	3
3. Secondary Optics .....	4
3.1 Pillow Lens Design .....	8
3.2 Reflector Design .....	11
3.3 Collimating Lens Design .....	15
4. Appendix 5A .....	18
4.1 Flux Integration of Rotationally Symmetric Radiation Patterns .....	18
About Lumileds .....	20

# 1. Optical Characteristics of SuperFlux LEDs

## 1.1 LED Light Output

The light output of an LED is typically described by two photometric measurements, flux and intensity.

In simple terms, *flux* describes the rate at which light energy is emitted from the LED. Total flux from an LED is the sum of the flux radiated in all directions. If the LED is placed at the center of a sphere, the total flux can be described as the sum of the light incident over the entire inside surface of the sphere. The symbol for photometric flux is  $\Phi_v$ , and the unit of measurement is the lumen (lm).

In simple terms, *intensity* describes the flux density at a position in space. Intensity is the flux per unit solid angle radiating from the LED source. The symbol for photometric intensity is  $I_v$ , and the unit of measurement is the candela (cd).

Solid angle is used to describe the amount of angular space subtended. Angular space is described in terms of area on a sphere. If a solid angle  $\omega$ , with its apex at the center of a sphere of radius  $r$ , subtends an area  $A$  on the surface of that sphere, then  $\omega = A/r^2$ . The units for solid angle are steradians (sr).

To put some of these concepts into perspective, consider the simple example of a candle. A candle has an intensity of approximately one candela. A candle placed in the center of a sphere radiates light in a fairly uniform manner over the entire inner surface ( $\omega = A/r^2 = 4\pi r^2/r^2 = 4\pi$  steradians). With this information, the flux from a candle can be calculated as shown below:

$$I_v = \frac{\Phi_v}{\omega}$$
$$\Phi_v = I_v \omega$$
$$\Phi_{v_{candle}} = 1 \text{ cd} \cdot 4\pi \text{ sr} \approx 12 \text{ lm}$$

## 1.2 SuperFlux LED Radiation Patterns

The radiation pattern of an LED describes how the flux is distributed in space. This is accomplished by defining the intensity of the LED as a function of angle from the optical axis.

Since the radiation pattern of most LEDs is rotationally symmetric about the optical axis, it can be described by a simple, two-axis graph of intensity versus angle from the optical axis. Intensity is normalized in order to describe the relative intensity at any angle. By normalizing intensity, the radiation pattern becomes a description of how the flux is distributed, independent of the amount of flux produced. Figure 5.1 shows a graph of the radiation pattern for an HPWA-Mx00 LED.

An attribute of the radiation pattern that is of common interest is known as the *full-width, half-max*, or  $2\theta_{1/2}$ . This attribute describes the full angular width of the radiation pattern at the half power, or half maximum intensity point. Looking at Figure 5.1, the  $2\theta_{1/2}$  of the HPWA-Mx00 LED is approximately  $90^\circ$ .

Another attribute that is of common interest is the *total included angle*, or  $\theta_{0.9}$ . This attribute describes the cone angle within which 90% of the total flux is radiated. Using Figure 5.1, the percent of total flux versus included angle can be calculated and graphed. (The derivation of this graph is shown in Appendix 5A.) This graph is included in the data sheet of SuperFlux LEDs and is shown in Figure 5.2 for the HPWA-Mx00 LED.

Looking at Figure 5.2, the total included angle is approximately  $95^\circ$ . This implies that 90% of the flux produced by an HPWA-Mx00 LED is emitted within a  $95^\circ$  cone centered on the optical axis.

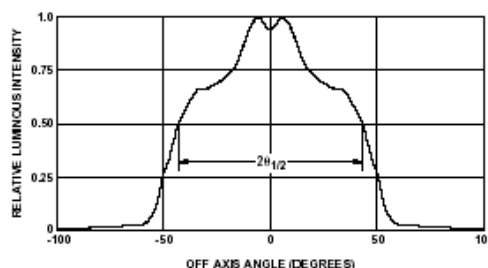


Figure 5.1 Graph of the radiation pattern for an HPWA-Mx00 LED.

## 2. Optical Modeling of SuperFlux LEDs

An optical model of the LED is useful when designing secondary optic elements such as reflector cavities and pillow lenses. The optical output of an LED can be approximated as a point source of light passing through an aperture, but modeling errors may be unacceptable when lenses or reflectors are placed within 25 mm of the SuperFlux LED. A more accurate technique involves using an optical model, which takes into account the extended source size of the LED.

### 2.1 Point Source Optical Model

The internal structure of a SuperFlux LED is shown in Figure 5.3. Light is produced in the LED chip. A portion of this light goes directly from the chip and is refracted by the epoxy dome (refracted-only light). The remainder of the light is reflected by the reflector cup and then refracted by the epoxy dome (reflected-refracted light).

The light that is refracted appears to come from a certain location within the LED, while the light which is reflected and refracted appears to come from a different location. In addition, because the LED chip itself has physical size and is not a point source, the refracted-only light does not appear to come from a single location, but a range of locations or a *focal smear*. This is true for the reflected-refracted light as well. These focal smears overlap, creating an elongated focal smear as shown in Figure 5.4.

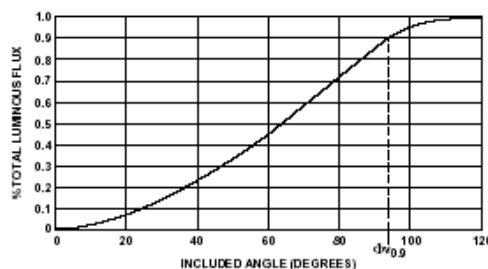


Figure 5.2 Percent total flux vs. included angle for an HPWA-MxOO LED.

To create the best approximation using a point source model, the center point of the focal smears should be chosen as the location of the point source; and the aperture size should be equal to that of the epoxy dome at its base as shown in Figure 5.5.

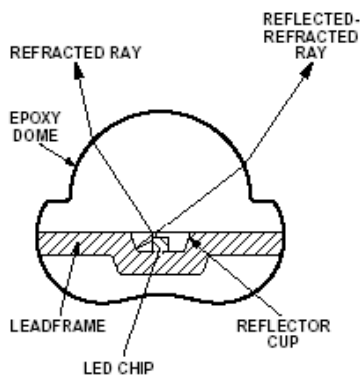


Figure 5.3 Internal structure of a SuperFlux LED.

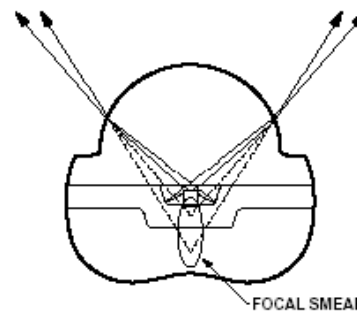


Figure 5.4 Focal smear produced by reflected and reflected-refracted light.

The optimal position of the point source for each SuperFlux LED is shown in Table 5.1.

### 2.2 Detailed Optical Models

Detailed optical models of LEDs include all the internal optical structures within the LED including the chip, the reflector, and the dome. In order to accurately construct such a model, detailed information about the chip, the reflector surface, and the epoxy encapsulant must be known. The process usually involves a tedious trial and error technique of changing parameters in the model until empirical measurements are matched.

Table 5.1 Position of Point Source for SuperFlux LEDs

SUPERFLUX LED PART NUMBER	POSITION OF POINT SOURCE "Z" (MM)
HPWA-Mx00	1.03
HPWA-Dx00	1.13
HPWT-Mx00	0.99
HPWT-Dx00	1.17

Due to the complexity of this process, Lumileds Lighting provides customers with rayset files for SuperFlux LEDs. The raysets contain spacial and angular information on a set of rays exiting the device at the dome surface. These raysets can be used by many optical-modeling software packages. Contact your local Lumileds Applications Engineer for more information and copies of the raysets.

### 3. Secondary Optics

This section contains practical design tools for secondary optic design. More accurate and sophisticated techniques exist which are beyond the scope of this application note. The design methods discussed here are proven, but no analytical technique can completely replace empirical testing. Designs should always be prototyped and tested as early in the design process as possible.

Secondary optics are used to modify the output beam of the LED such that the output beam of the finished signal lamp will efficiently meet the desired photometric specification. In addition, secondary optics serve an aesthetic purpose by determining the lit and unlit appearance of the signal lamp. The primary optic is included in the LED package, and the secondary optics are part of the finished signal lamp. There are two primary categories of secondary optics used, those that spread the incoming light (diverging optics), and those that gather the incoming light into a collimated beam (collimating optics).

The most common type of diverging optic used in automotive signal lamp applications is the pillow lens. The pillow lens spreads the incoming light into a more divergent beam pattern, and it breaks up the appearance of the source resulting in a more uniform appearance. A cross section of an LED signal lamp with a pillow lens is shown in Figure 5.6.

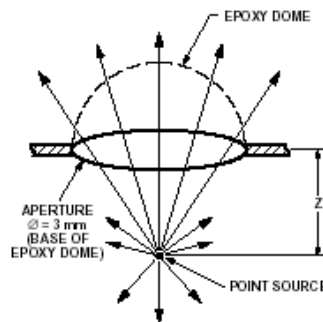


Figure 5.5 Point source model of a SuperFlux LED.

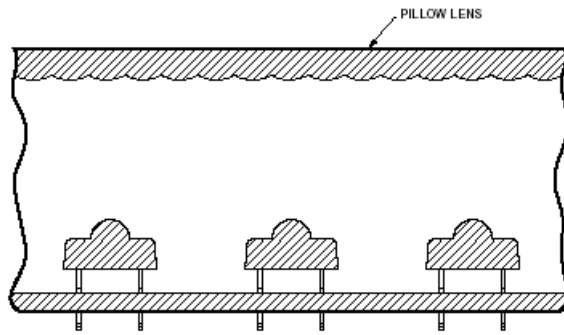


Figure 5.6 Cross section of an LED signal lamp with a pillow lens.

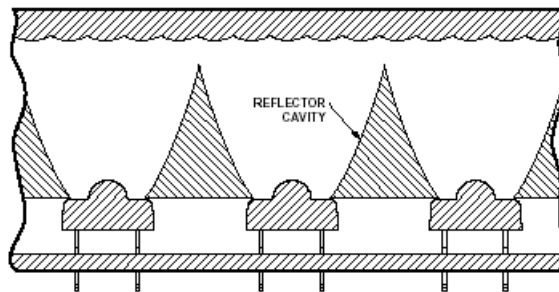


Figure 5.7 Cross section of an LED signal lamp with a reflector cavity and pillow lens.

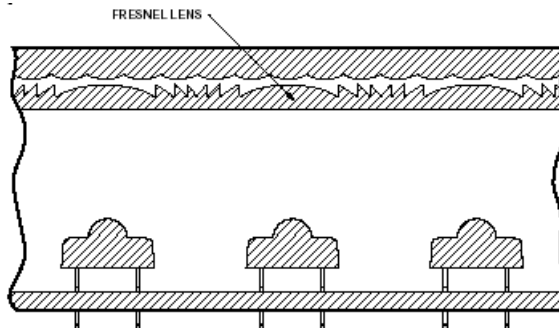


Figure 5.8 Cross section of an LED signal lamp with Fresnel and pillow lenses.

As the spacing between the pillow and the LEDs is increased, each LED will illuminate a larger area of the pillow lens. As the spot illuminated by each LED grows and as the adjacent spots begin to overlap, the lens will appear more evenly illuminated. The trade-off between lamp depth and lit uniformity is a common consideration in LED design, where both unique appearance and space-saving packages are desired.

Collimating optics come in two main varieties: reflecting and refracting. Reflecting elements are typically metalized cavities with a straight or parabolic profile. A cross section of an LED signal lamp with a reflector cavity and a pillow lens is shown in Figure 5.7.

Refracting, collimating optics typically used in LED signal lamp applications include plano-convex, dual-convex, and collapsed plano-convex (Fresnel) lenses. A cross section of an LED signal lamp with a Fresnel lens and a pillow lens is shown in Figure 5.8.

In general, designs that use collimating secondary optics are more efficient, and produce a more uniform lit appearance than designs utilizing only pillow or other non-collimating optics. Fresnel lenses are a good choice for thin lamp designs and produce a very uniform lit appearance. Reflectors are a good choice for thicker lamp designs and are more efficient than Fresnel lenses at illuminating non-circular areas. This is because reflectors gather all of the light, which is emitted as

a circular pattern for most SuperFlux LEDs, and redirect it into the desired shape. In addition, reflectors can be used to create a unique, "jeweled" appearance in both the on and off states.

The dependency of reflector height on reflector efficiency will be covered later in this section.

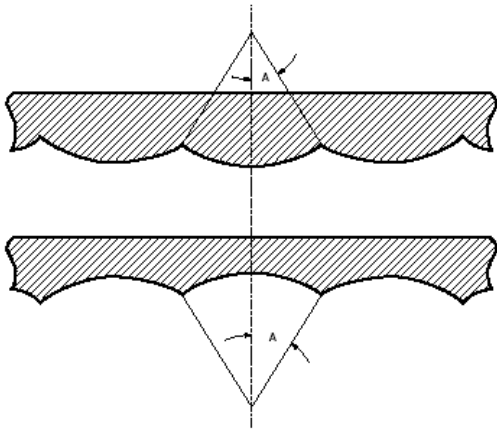


Figure 5.9 Half-angle subtended by an individual pillow (A) for convex (upper) and concave (lower) pillow lenses.

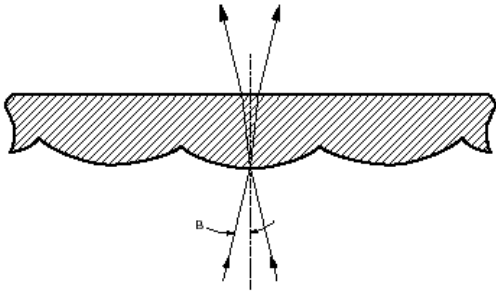


Figure 5.10 Half-angle divergence of the input beam (B).

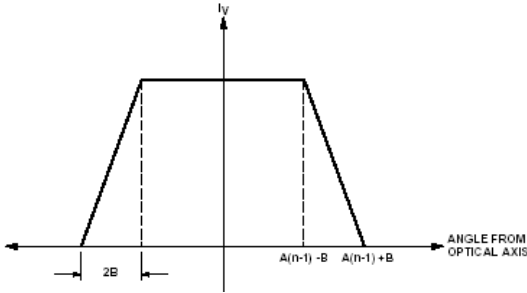


Figure 5.11 Ideal radiation pattern produced by a pillow optic where  $A(n-1) > B$ .

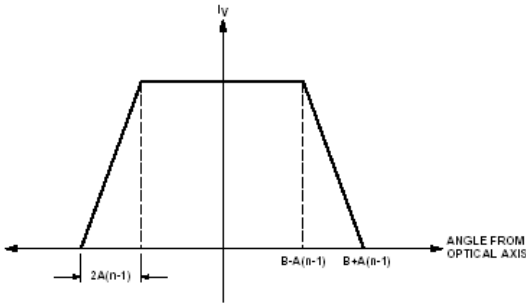


Figure 5.12 Ideal radiation pattern produced by a pillow optic where  $A(n-1) < B$ .

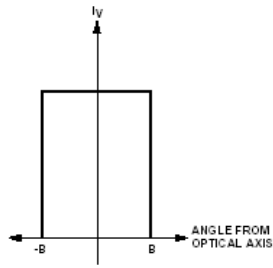


Figure 5.13 Ideal input beam with half-angle divergence B.

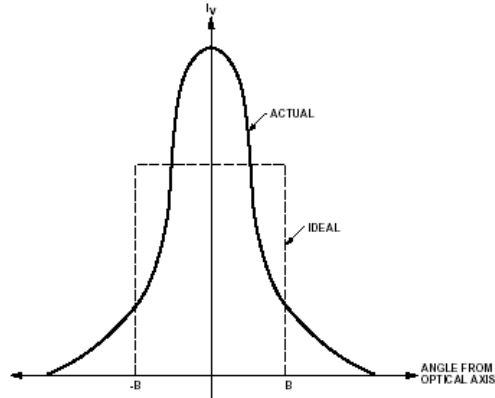


Figure 5.14 Common form of the input beam with half-angle divergence B.

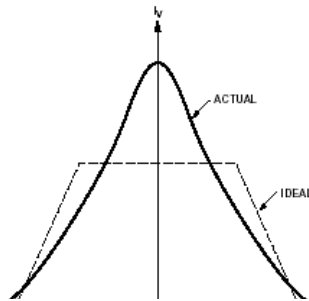


Figure 5.15 Ideal vs. actual radiation patterns from a pillow lens.

Table 5.2 CHMSL Intensity Specification

VERTICAL TEST POINTS (DEGREES)	MINIMUM LUMINOUS INTENSITY (CD)				
<b>10 U</b>	<b>8</b>		16		<b>8</b>
<b>5 U</b>	<b>16</b>	<b>25</b>	25	<b>25</b>	<b>16</b>
<b>H</b>	16	25	25	25	16
<b>5 D</b>	<b>16</b>	<b>25</b>	25	<b>25</b>	<b>16</b>
<b>Horizontal Test Points degrees)</b>	<b>10 L</b>	<b>5 L</b>	<b>V</b>	<b>5 R</b>	<b>10 R</b>

### 3.1 Pillow Lens Design

Consider a pillow lens where the half-angle subtended by an individual pillow is  $A$  as shown in Figure 5.9, and the input beam has a half-angle divergence  $B$  as shown in Figure 5.10.

The ideal radiation pattern generated would be as shown in Figure 5.11, where  $n$  is the index of refraction of the pillow lens material. It should be noted that Figure 5.11 is applicable when  $B$  is smaller than  $A(n-1)$ . This assumption is true for most LED applications using a collimating secondary optic.

In cases where  $B$  is larger than  $A(n-1)$ , which is often the case when the LED is used without a collimating optic, the ideal radiation pattern would be as shown in Figure 5.12.

The ideal radiation patterns shown in Figures 5.11 and 5.12 assume that the input beam has a box-like radiation pattern as shown in Figure 5.13.

However, in actual cases the input beam will have the characteristics of the Cosine form of the Lambertian as shown in Figure 5.14.

The differences between the ideal, box-like input beam, and the more common Lambertian input beam result in changes to the final radiation pattern as shown in Figure 5.15. The magnitude of this deviation in the radiation pattern can be estimated by evaluating the magnitude of the input beam's deviation from the ideal. This deviation from the ideal should be considered in the design of the pillow lens.

### 3.2 Design Case—Pillow Design for an LED CHMSL

Using a Center High Mounted Stop Lamp (CHMSL) as an example, we can see how the design techniques discussed previously can be used to determine an optimum value of  $A$ . The minimum intensity values for a CHMSL are shown in Table 5.2.

As a conservative estimate, we can treat this pattern as symmetric about the most extreme points. The extreme points are those with the highest specified intensity values at the largest angular displacements from the center of the pattern. These points are shown in italics in Table 5.2. The angular displacement of a point from the center is found by taking the square root of the sum of the squares of the angular displacements in the vertical and horizontal directions. A point at 10R and 5U would have an angular displacement from the center of:

$$\sqrt{(5^\circ)^2 + (10^\circ)^2} = 11^\circ$$

These points are charted on an intensity versus angle plot in Figure 5.16.

Consider the case where a collimating secondary optic is used producing a beam divergence of  $B = 5^\circ$  ( $B < A(n-1)$ ) and similar to that shown in Figure 5.14. The pillow lens material is Polycarbonate which has an index of refraction of 1.59 ( $n = 1.59$ ). The ideal CHMSL radiation pattern is shown in Figure 5.17 such that all the extreme points of the specification are satisfied. Figure 5.17 shows the predicted actual radiation pattern.

From Figure 5.17, we can see that  $A(n-1)-B = 8^\circ$  and  $A(n-1)+B = 18^\circ$ ; therefore,  $A = 22^\circ$ . *The value of  $A$  selected will determine how much spread the pillow optic adds to the input beam.*

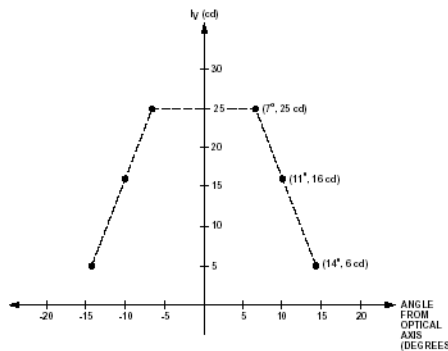


Figure 5.16 Extreme points on the CHMSL specification.

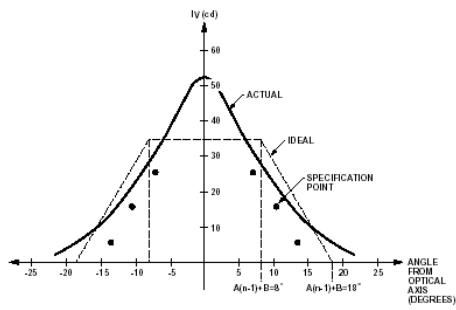


Figure 5.17 Ideal and actual radiation patterns satisfying the extreme points of the CHMSL specifications.

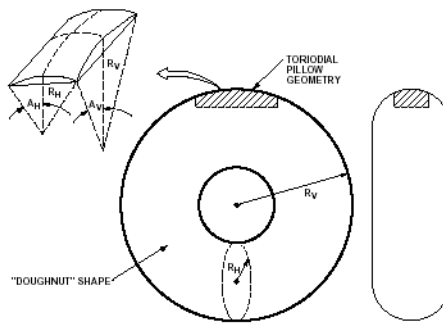


Figure 5.18 Toroidal pillow geometry.

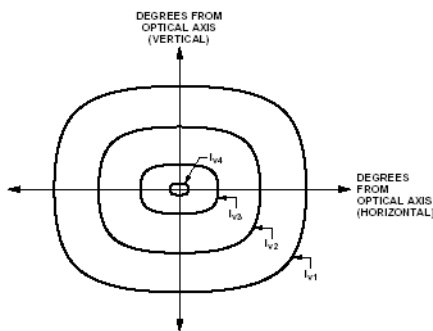


Figure 5.19 Radiation pattern produced by a toroidal pillow (determine  $A_V < A_H$ )

### Non-symmetric Pillow Lenses

In our previous example, the CHMSL radiation pattern was treated as if it were symmetric about its center. In this case, the radii of the pillow were the same along the horizontal and vertical axes, resulting in a spherical pillow.

In some signal lamps, the desired output beam is much wider along the horizontal axis than along the vertical axis. In these cases, the optimum value of  $A$  will be larger for the horizontal axis ( $A_H$ ) than the vertical axis ( $A_V$ ). The resulting geometry would be that of a circular toroid, which can be visualized as a rectangular piece cut from a doughnut as shown in Figure 5.18.

For non-symmetric pillow designs, an exercise similar to that performed for the CHMSL example must be performed for both the vertical and horizontal axes in order to determine  $A_V$  and  $A_H$ . The resulting isocandela plot of the radiation pattern will appear as shown in Figure 5.19.

### Selecting the Size of the Pillow Optic

After determining  $A$  for both axes, the next step is to determine the size, or pitch of the pillows. The pitch of the pillow typically does not effect performance, provided the individual pillows are small relative to the area illuminated by the light

source. For incandescent designs, this is not an issue and aesthetic considerations dictate the pillow size. However, for LED designs, the light source is an array of individual LEDs. The pillow lens pitch must be small relative to the area illuminated by a single LED or the pillow will not behave as designed. For this reason, pillows designed for LED applications typically have a pitch of 1 to 5 mm; where those designed for incandescents can be as large as 10 mm.

Figure 5.20 shows a top view of a single pillow with the pitches along both the horizontal,  $P_H$ , and vertical,  $P_V$ , axes. In addition, the cross-section geometry through the center of the primary axes is shown.

After  $A_H$  and  $A_V$  have been calculated, and the pitch has been chosen along one axis; the radii,  $R$ , and pitch along the other axis can be determined by using the following equations: (Note:  $P_H$  was chosen as a known value for this example.)

$$R_H = \frac{P_H}{2 \sin A_H}$$

$$y = R_H (1 - \cos A_H)$$

$$R_V = \frac{y}{1 - \cos A_V}$$

$$P_V = R_V (2 \sin A_V)$$

### Recommended Pillow Lens Prescriptions

Table 5.3 lists recommended pillow prescriptions ( $A_H$  &  $A_V$ ) for different signal lamp applications. The pitch can be changed to suit by varying  $R$  as described in the previous section.

Examining Table 5.3, we observe that for CHMSL designs, a symmetric pillow prescription was chosen ( $A_H = A_V$ ). However, for the rear combination lamp/front turn signal (RCL/FTS) application utilizing a collimating optic, a non-symmetric pillow prescription was used ( $A_H > A_V$ ). The desired output beam pattern for the RCL/FTS applications is twice as wide in the horizontal than in the vertical; whereas in the case of the CHMSL, the desired output beam is the same in the vertical and horizontal. In addition, for applications where no collimating secondary optic is used, the function of the pillow is to break up the appearance of the sources rather than spread the output beam. In these cases, a weak, symmetric prescription pillow was chosen.

The technique described above provides some practical tools for designing pillow lenses. If optical modeling software is available, along with an accurate model of the LED source, these tools should be utilized to aid in the design process and provide more accurate models of the final output beam.

Table 5.3 Recommended Pillow Lens Prescriptions

APPLICATION	LED TYPE	COLLIMATING OPTIC	$A_H$ (deg)	$A_V$ (deg)	$R_H$ (mm)	$P_H$ (mm)	$R_V$ (mm)	$P_V$ (mm)
CHMSL	HPWA-MHOO	Fresnel Lens ( $B = 5^\circ$ )	22	22	5.3	4	5.3	4
CHMSL	HPWT-DHOO	None ( $B = 20^\circ$ )	5	5	17	3	17	3
RCL/FTS	HPWT-MxOO	Fresnel Lens ( $B = 7^\circ$ )	30	20	4.0	4	8.9	5.7
RCL/FTS	HPWT-MxOO	Reflector Cavity ( $B = 20^\circ$ )	5	5	17	3	17	3

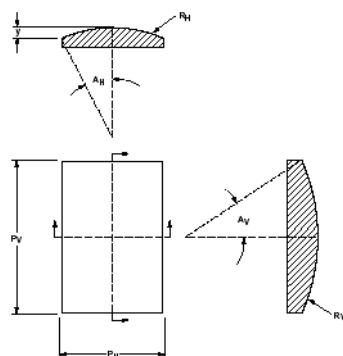


Figure 5.20 Geometry of a single pillow.

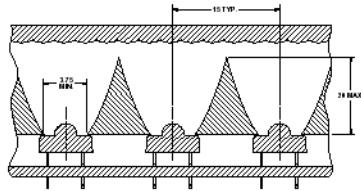


Figure 5.21 Cross-section geometry of a desired reflector cavity.

### Other Diverging Optics

Pillow lenses are the most popular diverging optic used in automotive signal lamps, however, other types exist which produce similar effects but have different appearances. Alternate types of diverging optics include: diffuse lenses, faceted lenses, rod lenses, and many others including combinations of the above. For example, diffuse lenses produce a uniform lit appearance and a cloudy unlit appearance. Pillow lenses can be diffused by bead-blasting the pillow lens surface on the mold tool resulting in a less efficient optic, but one that is more uniform in appearance when lit.

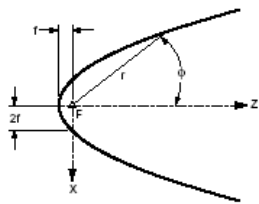


Figure 5.22 Geometry of a parabola.

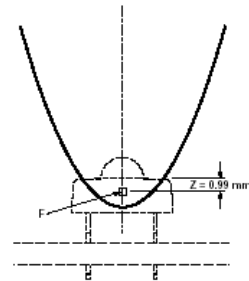


Figure 5.23 LED position relative to the parabola.

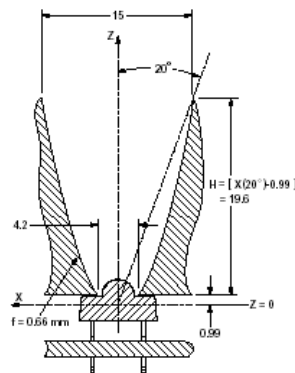


Figure 5.24 Design of parabolic reflector with  $f = 0.66$  mm.

## 3.2 Reflector Design

Reflector cavities serve two main purposes: to redirect the light from the LED into a useful beam pattern, and to provide a unique appearance for the finished lamp. Often the look sought after is not achievable by the most optically efficient design. As a result, there is a trade-off required between optical efficiency and lit appearance to arrive at an acceptable design.

As discussed in the previous section *Point Source Optical Model*, a parabola is designed to collimate the light from the point source. For the design technique discussed here, the LED is treated as a point source. This treatment is very accurate for larger parabolas where the size of the dome is small relative to the exit aperture of the reflector. Once the parabola has been designed, a cavity with a profile comprised of multiple linear sections that closely approximates the form of the parabola may be used depending on the look desired.

In order to accommodate the SuperFlux LED dome, the bottom aperture of the reflector must be greater than three-millimeters in diameter. Considering the tolerances of the molded reflector, the LED, the LED alignment to the PCB, and

the alignment of the reflector to the PCB, the bottom reflector aperture should be a minimum of 3.5 mm in diameter. The focal length of the reflector must be greater than 0.5 mm to produce a bottom aperture of greater than 3.5 mm.

### Design Case—Reflector for a CHMSL Application

Consider the case where a reflector cavity will be used to collimate the light from an HPWT-MH00 source, and a pillow optic cover lens will be used to form the final radiation pattern. Vacuum-metalized ABS plastic will be used as the reflector material. The reflector cavity can be a maximum of 20 mm in height and should have a minimum opening for the LED dome of diameter 3.75mm to accommodate piece-part misalignment and tolerances. The LED spacing is 15 mm, and each cell must illuminate a 15 mm x 15 mm patch on the pillow lens. Figure 5.21 shows a cross-section of the lamp described above. The geometry of a parabola, in polar coordinates, is described by the following equation:

$$r = \frac{2f}{(1 - \cos\phi)}$$

Figure 5.22 shows how the terms in this equation are applied.

From Table 5.1, we find that the optimum point source location for the HPWT-MH00 LED is at  $Z = 0.99$  mm. Placing the point source of the LED at the focus of the parabola will result in an LED position as shown in Figure 5.23.

Since the base of the LED dome is above the location of the parabola's focus, this implies that  $2f < 1/2$  base aperture =  $3.75 \text{ mm}/2 = 1.875 \text{ mm}$  ( $f < 0.94 \text{ mm}$ ). This information will give us a starting point to begin searching for the optimum parabola.

Table 5.4 describes the profiles of three different parabolas ( $f = 0.9 \text{ mm}, 0.7 \text{ mm}, 0.66 \text{ mm}$ ).

An efficient, practical collimator design for a CHMSL application should collimate all the light beyond  $20^\circ$  from on axis ( $\Phi \leq 20^\circ$ ). More efficient reflectors can be designed which collimate more of the light, but they are typically too deep to be of practical value.

The ideal reflector for this application will have the following characteristics:

*Height constraint:*  $0.99 \leq z \leq 20 \text{ mm}$

*Fit of LED dome into bottom aperture:*  $x(z = 0.99 \text{ mm}) \geq 1.875 \text{ mm}$

*15 mm pitch:*  $x(\Phi = 20^\circ) \cong 7.5 \text{ mm}$

Looking at Table 5.4, we find that the parabola with  $f = 0.66 \text{ mm}$  most closely meets these requirements. Figure 5.24 gives the geometry of the parabolic reflector chosen.

Figure 5.25 shows the profiles of several practical reflector geometries ( $f = 0.5$  to  $1.0 \text{ mm}$ ). It should be noted that in order to produce a reflector with a cutoff angle less than  $20^\circ$ , the height must increase radically. For this reason, reflectors with a high degree of collimation ( $<20^\circ$ ) are often impractical. Therefore, Fresnel lenses are the preferred method to produce highly collimated beams. In addition, it can be seen that reflectors with smaller focal lengths can produce a greater degree of collimation in a shorter height, however, the exit aperture also becomes smaller.

### Reflector Cavities with Linear Profiles

After designing the appropriate parabolic reflector, this form can be closely approximated by a few linear sections. Reflectors with linear profiles require simpler mold tools and are easier to measure and verify the accuracy of the form. Usually two linear sections are sufficient depending on the efficiency needed and the appearance that is sought. Figure 5.26 shows an approximation of the parabolic reflector from the previous section, designed by a best fit of two linear sections.

### Reflector Cavities with Square and Rectangular Exit Apertures

The previous sections dealt with reflector cavities that are rotationally symmetric about the optical axis, which result in round entrance and exit apertures. In some designs, it may be desirable to have a square or rectangular exit aperture in order to more evenly illuminate a square or rectangular section of the cover lens. In this type of design, each axis of the reflector cavity must be analyzed separately, using the techniques described in the previous section.

It should be noted that these reflector cavities will produce beam patterns that are similar in shape to their exit aperture. Figure 5.27 compares the beam patterns of the rotationally-symmetric parabolic reflector designed in the previous example *Design Case—Reflector for a CHMSL Application* to that of a reflector cavity with a square exit aperture having the

same wall profile. In this case, each side of the square exit aperture is equal in length to the diameter of the circular exit aperture of the parabolic design.

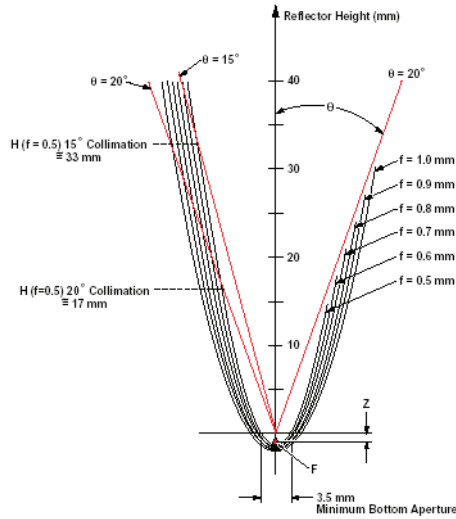


Figure 5.25 Comparison of Practical Parabolic Reflector Profiles.

### Other Reflector Design Techniques

Many other methods exist to design reflectors for LED sources.

Nonimaging techniques focus on extracting light from the LED source and redirecting it such that the exit beam has the desired divergence. The most common form of a Nonimaging reflector used for LED applications is a truncated, compound parabolic collector (CPC). Several publications explaining the principles of Nonimaging optics exist. One such text is *High Collection Nonimaging Optics* by Welford & Winston, 1989.

Other reflector design techniques have been developed by William B. Elmer. One concept of particular interest is a method for designing rotationally symmetric reflectors by mapping the flux contained within the source beam into the desired output beam. This method breaks the input beam into angular sections, each containing a known percentage of the total flux. It is then determined at what angle each of these flux packets should be reflected to produce the desired output beam. The profile of the final reflector will consist of a series of straight sections. As the number of flux packets considered is increased, the number of steps in the reflector increases, until a smooth curve is approximated.

Detailed information on the reflector design principles developed by William Elmer can be found in *The Optical Design of Reflectors* by William Elmer, 1989.

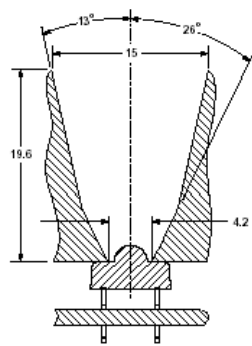


Figure 5.26 Linear profile approximation of a parabolic reflector ( $f = 0.66$  mm).

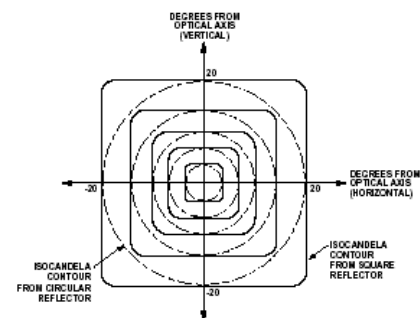


Figure 5.27 Isocandela plots of a circular vs. square reflector design.

Table 5.4 Profile Geometry of Parabolas (f = 0.9 mm, 0.7 mm, 0.66mm)

f (mm)	$\Phi$ (deg.)	$\Phi$ (rad.)	R (mm)	X (mm)	Z (mm)
<b>0.9</b>	20	0.35	29.85	10.21	28.05
	22	0.38	24.72	9.26	22.92
	25	0.44	19.21	8.12	17.41
	30	0.52	13.44	6.72	11.64
	35	0.61	9.95	5.71	8.15
	40	0.70	7.69	4.95	5.89
	45	0.79	6.15	4.35	4.35
	50	0.87	5.04	3.86	3.24
	55	0.96	4.22	3.46	2.42
	60	1.05	3.60	3.12	1.80
	65	1.13	3.12	2.83	1.32
70	1.22	2.74	2.57	0.94	
<b>0.70</b>	20	0.35	23.21	7.94	21.81
	22	0.38	19.23	7.20	17.83
	25	0.44	14.94	6.31	13.54
	30	0.52	10.45	5.22	9.05
	35	0.61	7.74	4.44	6.34
	40	0.70	5.98	3.85	4.58
	45	0.79	4.78	3.38	3.38
	50	0.87	3.92	3.00	2.52
	55	0.96	3.28	2.69	1.88
	60	1.05	2.80	2.42	1.40
	65	1.13	2.42	2.20	1.02
70	1.22	2.13	2.00	0.73	
<b>0.66</b>	20	0.35	21.89	7.49	20.57
	22	0.38	18.13	6.79	16.81
	25	0.44	14.09	5.95	12.77
	30	0.52	9.85	4.93	8.53
	35	0.61	7.30	4.19	5.98
	40	0.70	5.64	3.63	4.32
	45	0.79	4.51	3.19	3.19
	50	0.87	3.70	2.83	2.38
	55	0.96	3.10	2.54	1.78
	60	1.05	2.64	2.29	1.32
	65	1.13	2.29	2.07	0.97
70	1.22	2.01	1.89	0.69	

### 3.3 Collimating Lens Design

In this section we will deal with spherical lenses and geometrical optics design techniques, treating the LED as a point source of light. More sophisticated and accurate methods exist, but are beyond the scope of this application note.

An LED signal lamp with a dual-convex, collimator lens is shown in Figure 5.28. The “lensmaker’s” formula for this arrangement is shown below:

Where:

$$\frac{1}{f} = (n-1) \left[ \frac{1}{R_1} + \frac{1}{R_2} \right]$$

$f$  = focal length of the lens

$n$  = index of refraction of the lens material

$R_1$  = radius of lens surface nearest the LED

$R_2$  = radius of other lens surface

$T$  = thickness of the lens

If  $T$  is less than one sixth of the diameter of the lens, then this equation simplifies to:

$$\frac{1}{f} = (n-1) \left[ \frac{1}{R_2} \right]$$

For thin lenses, it is a good approximation to measure  $f$  from the center of the lens.

For thin, plano-convex lenses ( $R_1 = \infty$ ), the equation further simplifies to:

The above equations assume all rays arrive at shallow angles with respect to the optical axis (paraxial assumption).

However, for SuperFlux LED applications, where much of the flux is contained at angles far from the optical axis, this is not the case. As a result, rays which are not close to the optical axis will be bent at too great an angle, a condition known as *spherical aberration*. A correction factor,  $C$ , can be added to the above equations to compensate for this effect as shown below:

$$\frac{1}{f} = C(n-1) \left[ \frac{1}{R_1} + \frac{1}{R_2} \right]$$

For most LED collimator designs, a correction factor of  $C \cong 1.35$  will produce the best results. The value of  $f$  chosen can be checked by tracing a ray from the source to the outer edge of the collimator lens (edge ray). If the edge ray is under collimated, the value of  $C$  used is too large. If the edge ray is over collimated, the value of  $C$  used is too small. Figure 5.29 graphically depicts the edge ray method for checking  $f$ .

#### Fresnel Lens Design

A Fresnel lens can be visualized as a thick convex lens which has been collapsed about a series of circular, stepped setbacks. This type of lens takes on the properties of a much thicker lens and eliminates the difficulties involved with the manufacture of thick lenses.

A cross-section through the center of a plano-convex lens, and its Fresnel counterpart are shown in Figure 5.32.

The thickness of the Fresnel lens is reduced as the number of steps is increased. Typically Fresnel lenses are designed with the minimum number of steps needed to achieve the desired thickness, because additional light losses may occur at the internal faces and joining vertices. However, for plastic lenses, a thin design is desirable where excessive lens thickness will result in sink distortions. Therefore, the performance and moldability of a lens are traded-off when choosing the optimal number of steps.

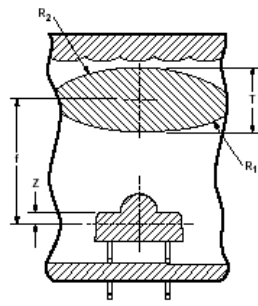


Figure 5.28 Cross-section of an LED signal lamp using a dual-convex, collimator lens.

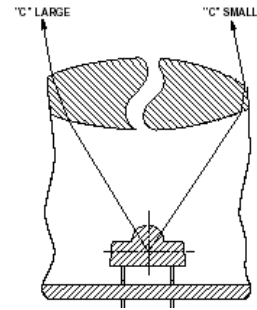


Figure 5.29 Edge ray method for checking  $f$ .

### Design Case—Collimator Lens

Consider the case where a lens will be used to collimate the light from an HPWT-DH00 source, and a pillow optic cover lens will be used to form the final radiation pattern. Clear PMMA ( $n = 1.49$ ) will be used as the lens material. The LED spacing is 20 mm and the spacing from the top of the PCB to the top surface of the lens must be less than 25 mm.

The total included angle of the HPWT-DH00 is  $70^\circ$ , therefore, to capture 90% of the light from the LED, the lens must span  $35^\circ$  from the optical axis, and fill a 20 mm X 20 mm area. The combination of included angle, lamp depth, and LED spacing define the necessary items to determine  $f$ . Figure 5.30 shows a cross-section of the lamp described above.

Examining the geometry shown in Figure 5.30, the desired focal length,  $f$ , is approximately 15.3mm. A lens of this power will be a dual-convex, and  $R_1$  and  $R_2$  can now be calculated using the following equation:

To optimize collection efficiency,  $R_1$  must be greater than  $R_2$ . By placing the flatter surface closer to the LED, the ray bending is more equally shared between the two lens surfaces. However, if  $R_2$  becomes too small, the lens will be too thick and difficult to manufacture. A good compromise between these two competing factors is  $R_1 = 24$  mm, and  $R_2 = 18$  mm. Figure 5.31 shows a cross-section of an LED signal lamp with this dual-convex lens design.

$$\frac{1}{15.3} = 1.35(1.5 - 1) \left[ \frac{1}{R_1} + \frac{1}{R_2} \right]$$

$$\therefore \frac{R_1 R_2}{R_1 + R_2} = 10.3 \text{ mm}$$

Consider a case with a plano-convex lens ( $R = 19$ mm) where an aperture diameter of 25 mm is desired for use as a collimating lens. This lens will be too thick to properly injection mold (greater than 6 mm), so a Fresnel design will be used with a maximum height of 4 mm. The resulting design will have three steps, as shown in Figure 5.32.

Convex-Fresnel lenses can be designed in which a large radius (low curvature) lens is used on the LED side, and a Fresnel-type lens with a smaller radius (more curvature) is used on the other side as shown in Figure 5.33.

### Other Lens Design Options

In this section we have discussed only spherical lens designs. Spherical lenses are easily designed, specified, and checked; but may not be the most efficient collimator due to spherical aberrations. Other lens designs, such as hyperbolic-planar, sphero-elliptic, and free-form lenses can be designed which may be more efficient than spherical forms. However, the design of these types of lenses is more complex and generally requires optical modeling software and accurate optical models of the LED.

Another class of lens exists which couple the principles of refraction and total internal reflection (TIR). These lenses are commonly referred to as reflective/refractive, or catadioptric lenses. Lenses designed by Fresnel over 100 years ago for light houses contained such TIR faces for improved efficiency. An example of a catadioptric lens is shown in Figure 5.34.

This type of lens is useful when refractive lens designs cannot efficiently bend the light rays at the required angle. By combining reflection and refraction into a single optical element, a very powerful and efficient lens can be designed. TIR is most efficient when incident rays are nearly tangential, where as refraction is most efficient when the rays are close to the normal.

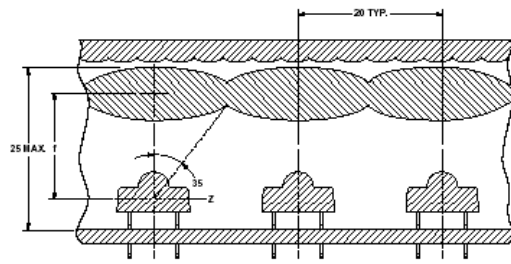


Figure 5.30 Cross-section of the desired LED lamp configuration.

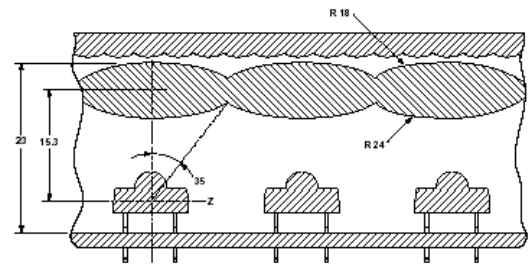


Figure 5.31 Cross-section of an LED signal lamp with a dual convex lens ( $R1 = 24\text{mm}$ ,  $R2 = 18\text{mm}$ ).

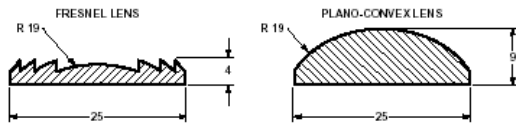


Figure 5.32 Cross-section of a plano-convex lens and its Fresnel equivalent.

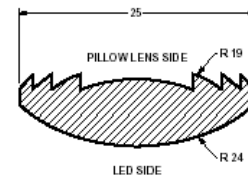


Figure 5.33 Convex-Fresnel lens used as an LED collimator.

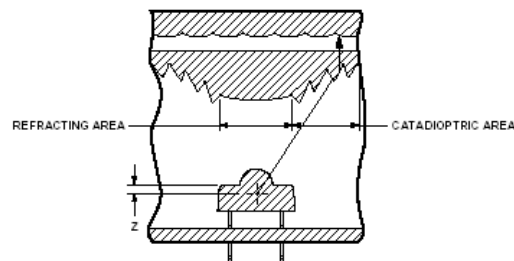


Figure 5.34 Cross-section of a catadioptric lens used as an LED collimator.

## 4. Appendix 5A

### 4.1 Flux Integration of Rotationally Symmetric Radiation Patterns

The cumulative flux as a function of angle from the optical axis (Figure 5.2) can be calculated from the radiation pattern (Figure 5.1). This calculation is simple for rotationally symmetric radiation patterns and is shown below:

Intensity is defined as the flux per unit solid angle, or

$$I_{\theta} = \frac{\Phi_{\theta}}{\omega} \quad (1)$$

This equation can be rearranged to solve for flux.

$$\Phi_{\theta} = I_{\theta} \omega \quad (2)$$

$$\Phi_{\theta} = \int I_{\theta} d\omega \quad (3)$$

Solid angle,  $\omega$  as a function of  $\theta$  can be determined with the aid of Figure 5A.1.

$$d\omega(\theta) = 2\pi r \sin\theta d\theta \quad (4)$$

Assigning a value of  $r=1$ , this equation becomes

$$d\omega(\theta) = 2\pi \sin\theta d\theta \quad (4)$$

and substituting (5) into (3) we can solve for  $\Phi_{\theta}(\theta)$

$$\Phi_{\theta}(\theta) = 2\pi \int I_{\theta}(\theta) \sin\theta d\theta \quad (6)$$

Consider the case where the LED has a rotationally symmetric, lambertian radiation pattern as shown in the Figure 5A.2.

Substituting  $I_{\theta}(\theta)$  into (6) we get:

$$\begin{aligned} \Phi_{\theta}(\theta) &= 2\pi \int \cos\theta \sin\theta d\theta \quad (7) \\ &= \pi \sin^2\theta \end{aligned}$$

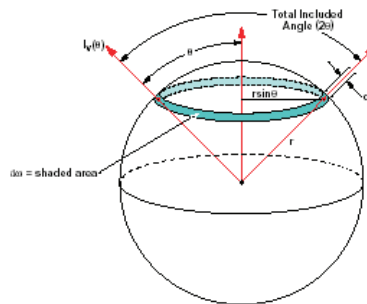


Figure 5A.1 Graphic explanation of flux integration technique.

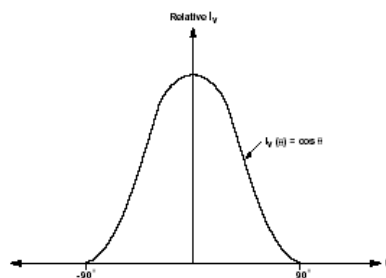


Figure 5A.2 Rotationally symmetric, lambertian radiation pattern.

The plot for equation (7) is shown in Figure 5A.3.

By normalizing the Y-axis to 100% at 90°, this graph becomes that which is typically shown in the LED data sheets (Figure 5A.4). It should be noted that the data sheet refers to the X-axis as “Total Included Angle” which is equal to  $2\theta$  (see Figure 5A.1).

For rotationally symmetric radiation patterns that cannot be easily represented with functions, Simpson’s rule can be applied to approximate the integral. For example, the HPWT-MH00 radiation pattern cannot be easily described by a function. In such a case, the radiation pattern can be divided into a finite number of elements each with an angular width,  $d\theta$ , as shown in Figure 5A.5.

The smaller the  $d\theta$  chosen, the larger  $n$  will become and the more accurate the approximation of the integral becomes. Applying Simpson’s rule, we can approximate (6) by the following summation

$$\Phi_{\theta}(\theta) = 2\pi \left[ \sum_0^n I_{\nu_n} \sin\theta \, d\theta \right] \quad (8)$$

As before, (8) can be plotted as shown in Figure 5A.6.



Figure 5A.4 Percent cumulative flux vs. total included angle.

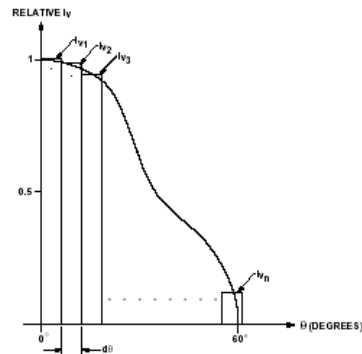


Figure 5A.5 Approximation of the HPWT-MH00 radiation pattern.

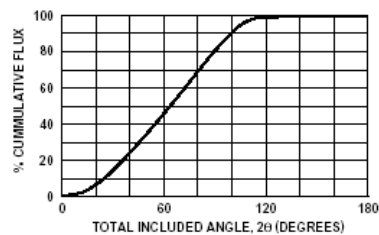


Figure 5A.6 Graphic representation of equation (8).

## About Lumileds

Lumileds is the light engine leader, delivering innovation, quality, and reliability.

For 100 years, Lumileds commitment to innovation has helped customers pioneer breakthrough products in the automotive, consumer and illumination markets.

Lumileds is shaping the future of light with our LEDs and automotive lamps, and helping our customers illuminate how people see the world around them.

To learn more about our portfolio of light engines visit [www.lumileds.com](http://www.lumileds.com).



©2015 Lumileds Holding B.V. All rights reserved.  
LUXEON is a registered trademark of the Lumileds Holding B.V.  
in the United States and other countries.

[www.lumileds.com](http://www.lumileds.com)

Neither Lumileds Holding B.V. nor its affiliates shall be liable for any kind of loss of data or any other damages, direct, indirect or consequential, resulting from the use of the provided information and data. Although Lumileds Holding B.V. and/or its affiliates have attempted to provide the most accurate information and data, the materials and services information and data are provided "as is," and neither Lumileds Holding B.V. nor its affiliates warrants or guarantees the contents and correctness of the provided information and data. Lumileds Holding B.V. and its affiliates reserve the right to make changes without notice. You as user agree to this disclaimer and user agreement with the download or use of the provided materials, information and data.